Molecular Dynamics Computer Simulations of Surfactant Monolayers: Monododecyl Pentaethylene Glycol at the Surface between Air and Water

Hubert Kuhn* and Heinz Rehage

University of Essen, Department of Environmental Chemistry, Universitaetsstrasse 3-5, D-45141 Essen, Germany

Received: February 17, 1999; In Final Form: June 17, 1999

In this publication we used molecular dynamics computer simulations in order to get a more detailed insight into the dynamic properties of monododecyl pentaethylene glycol ($C_{12}E_5$) monolayers at the water surface. We used a simulation box enclosing 36 surfactant molecules and the surfactant concentration was kept constant at an average value of 0.55 nm^2/molecule. After reaching the thermodynamic equilibrium, it turned out that the dodecyl chains were approximately oriented diagonal to the surface with an average value of about 43° measured in respect to the surface normal vector. This result is in fairly good agreement with a previously performed simulation containing only 25 surfactant molecules. The average orientation angle of the hydrophobic chains agrees very well with experimental data. In contrast to the unpolar part of the molecules the water-soluble glycol chains were aligned more perpendicular to the water surface with a tilt angle of only 11°. It is interesting to note that these chains are rather stiff. Within the time scale of our simulation the surfactant molecules were firmly attached at the surface and did not enter into the water phase. All alkyl and glycol chain ends, however, were characterized by a striking flexibility. The calculation of pair distribution functions and detailed pattern analysis of the oxygen atoms within the glycol chains revealed a pentagonal arrangement in the highly ordered internal segments of the E_5 chain.

Introduction

At the water surface alkyl glycol ether surfactants tend to form ultrathin monolayers due to the amphiphilic properties of these compounds. As the adsorption process is based on hydrophilic and hydrophobic forces, it can be expected that the polar glycol chains are dissolved in the water phase whereas the alkyl chains seek to avoid the energetically unfavorable contact with solvent molecules. As a consequence, hydrophilic and hydrophobic chains are randomly oriented in the vicinity of the water surface.

In several technical applications these effects are important since, for instance, in foams the amphiphilic films are used to stabilize the internal structures. It turns out that these systems are much influenced by physical parameters such as the interface or surface tension or the elasticity and curvature of the monolayer. Furthermore, it can be shown that molecular features of the adsorbed surfactant films determine these macroscopic parameters. Without going into further detail, we can expect that the orientation of surfactant chains and the conformation distribution in the alkyl and glycol ether chains have some influence on these parameters.

Much information on the structural and phase behavior of Langmuir monolayers has been obtained from experimental techniques such as fluorescence microscopy, small-angle X-ray scattering, and neutron diffraction. Neutron reflection experiments of tri-, hexa-, and octaethylene glycol monododecyl ether adsorbed at the air/water interface were already published.[1−3] Recently, neutron reflection results concerning the structure of $C_{12}E_5$ were also presented.[4] In these investigations new insights into structural details were obtained such as orientation and layer thickness of the alkyl and glycol ether chains. From these results it became clear that the unpolar chains are generally not oriented perpendicular to the surface. With decreasing surfactant concentration the tilt angle increased and in the regime of small concentrations the molecules were found to lie flat on the water surface.[1] Neutron reflection studies of monolayer systems of $C_{12}E_N$ ($N = 2-6, 8$) at surface concentrations of 0.55−0.65 nm^2/molecule revealed that the alkyl chain thickness does not depend very much on the nature of the polar headgroup.[3,4] Despite these results on the structure of surfactant monolayers, it is desirable to perform additional investigations to improve the knowledge on molecular self-assembling processes in thin films.

Over the last years a number of molecular dynamics simulations of surfactant monolayers have been published.[5−30] In these studies, the water surface was often modeled as a flat amorphous plane allowing only van der Waals interactions between the surfactant atoms and the planar surface.[5−21] For the calculation of atom−surface interactions, modified functional forms of Lennard-Jones potentials were frequently used.

Due to the high demanding computer performance for investigations of molecular films, there have been only few attempts in which the surface has been modeled in all atomic details.[22−30] Schweighofer et al. performed molecular dynamics simulations of sodium dodecyl sulfate at the water/vapor and the water/CCl_4 interface at low surface concentrations.[22] Böcker et al. simulated monolayers of hexadecyltrimethylammonium chloride at the air/water interface,[23] and a similar surfactant system was studied by Tarek et al., who investigated the properties of tetradecyltrimethylammonium bromide monolayers.[24] Furthermore, the structures of phenol and *p*-*n*-pentylphenol on water were simulated by Pohorille and Benjamin.[25−26] With Monte Carlo statistical mechanics Gao and Jorgensen examined

* To whom correspondence should be addressed. E-mail: hubert.kuhn@uni-essen.de. Phone: +49 (0)201-183-2868. Fax: +49 (0)201-183-3951.

10.1021/jp990595o CCC: $18.00
Published on Web 09/17/1999

the energy and structure for 1-hexanol/water mixtures in a monolayer.[27] Recently, the structural and dynamic properties of *N,N′*-diethyl-*p*-nitroaniline at the water interface were studied.[29]

However, for the simulation of extended glycol chains such as E_5 immersed in the water phase, it is necessary to consider the specific interactions between the hydrophilic chains and the surrounding solvent molecules. It is worthwhile to assume a great influence of hydrogen bonds on the molecular structure of the polar headgroups.

In a previous molecular dynamics simulation we investigated the orientation of glycol and hydrophobic alkyl chains of $C_{12}E_5$ on the air/water interface. In this work we constructed a model with 25 surfactants adsorbed on the water surface. Details of the simulation procedure and the results are given in ref 30. The calculated average orientation angles were in fairly good agreement with experimental data.[1−4] We have concluded from this that already 25 surfactants assembled on the water surface are sufficient to obtain reliable results for the examined molecular tilt angles.

In addition to our previous simulation, we extended the simulation model by increasing the number of adsorbed surfactants to 36 $C_{12}E_5$ molecules. Furthermore, the present work contains important new results. In this paper we focuss our attention on the molecular structure of the E_5 chains in the water phase. The molecular structure between the E_5 oxygens were investigated in detail. Also, we have analyzed and compared the mobility of the C_{12} and E_5 chains. These computer simulations provide new insights into the differences of the molecular structures of the alkyl and hydrophilic glycol chains. As far as we know, a molecular dynamics computer simulation of adsorbed alkyl glycol ether surfactants was never done before. It turns out that this type of investigation is especially useful for understanding the stability and the dynamic properties of ultrathin adsorbed films.

Method and Theory

We have investigated a microscopic part of a monolayer consisting of monododecyl pentaethylene glycol surfactants adsorbed at the water surface. The intra- and intermolecular interactions between all atoms were calculated with classical mechanics approximations. All potential functions and parameters were taken from the AMBER force field.[31−33] For calculation of the inter- and intramolecular energy functions for the solvent molecules, we used the SPC water parameters.[34] In our simulation all surfactant atoms and solvent molecules were included in the calculation of the atomic interactions.

The number of molecules, N, was composed of 36 surfactant and 1575 water molecules. Surfactants and water particles were arranged in a cubic box with periodic boundary conditions. The dimension of the simulation box was $L_x = L_y = 4.44$ nm and $L_z = 8.0$ nm. In the coordinate system the x and y axes were lying within the area of the water surface. The z axis was directed perpendicular to the surface. The application of the large L_z value was necessary in order to avoid additional interactions with the boundary box on top of the water surface.

In the SPC-model bond length and bond angle constraints were used to force these parameters to desired SPC parameter values. We also used intramolecular bond length constraints for the simulation of the surfactant molecules. The distances between bonded atoms were obtained from the minimum of the potential energy of a surfactant monomer in a vacuum. This calculation was performed with respect to all internal coordinates. For this procedure and all subsequent minimizations of the potential energy we used the steepest descent method in combination with the conjugate gradients Polak−Ribiere algorithm.[35] To apply the bond constraints in the molecular dynamics run, the RATTLE algorithm was used.[36] In contrast to the bond lengths constraints, all possible changes of bond angels and dihedrals in the surfactant molecules were allowed during the simulation run.

To truncate the range of the intermolecular van der Waals interactions and electrostatic forces, we used an minimum image model with an energy cutoff of 1 nm for both types of the interactions. Additionally, the nonbonded 1−4 interactions were scaled by 0.5. With the charge group approximation applied in the simulation, we ensured that no artificial dipole splits disturbed the calculation of the nonbonded electrostatic energy.

At the beginning of the simulation, the 36 surfactant molecules were arranged in such a way that the hydrophobic carbon chains were orientated in the z direction, parallel to the surface normal. Furthermore, the alkyl and glycol chains were generated in all-trans conformations and the polar glycol chains were completely surrounded by water molecules. Since the molecular arrangement of the water phase was based on a previous *NPT* equilibrium molecular dynamics simulation, the initial water density was equal to 1 g/cm^3. This calculation was performed in a periodic boundary box consitsting of 1000 SPC water molecules.

At the critical micelle concentration (cmc) we may suppose that the water surface is saturated by amphiphilic molecules. The area per surfactant molecule (A) at the cmc is a characteristic parameter for each type of surfactant. In our simulation, the surface area corresponded to a value of $A = 0.55$ nm^2/surfactant. $C_{12}E_5$ is well dissoluble in water with the effect that at the cmc the monolayer is saturated and tends to collapse. The micellization process starts and interactions between surfactant molecules adsorbed at the surface and dissolved monomers become dominant. To avoid these complications, we simulated the system below the cmc, where A is equal to 0.50 ± 0.03 nm^2/molecule.[4] Though this is a simplification, it is nevertheless interesting to investigate the influence of dissolved surfactants on the monolayer structure at and below the cmc.

In a first set of computer simulations the total potential energy of the system was minimized to generate an appropriate starting point for the dynamics simulation. After minimization, random velocities, according to a Gaussian distribution and a temperature of 298 K, were assigned to each atom. The temperature of the system was set to 298 K and remained constant during the simulation by direct velocity scaling. To integrate the Newtonian equations of motion for all atoms, we used the Verlet velocity integrator,[37] a variant of the Verlet leapfrog algorithm. With the introduction of bond length and bond angle constraints in combination with the RATTLE method, we were able to set the integration time step to 2 fs.

It is evident that the initially generated monolayer structure and the arrangement of water molecules in the simulation box are far away from the thermodynamic equilibrium. Therefore, during a 500 ps simulation we allow the system to equilibrate. Even after long simulation times we observed fluctuations of the total energy (sum of kinetic and potential energy) around a constant equilibrium value, which was identified as the average total energy. An additional 500 ps molecular dynamics simulation was performed for the final data collection run. Finally, monolayer structural data were obtained from averaging of the atomic Cartesian coordinates collected in this 500 ps simulation.

We performed the molecular dynamics calculation on an IBM-SP2-parallel computer with eight processors. The trajectory

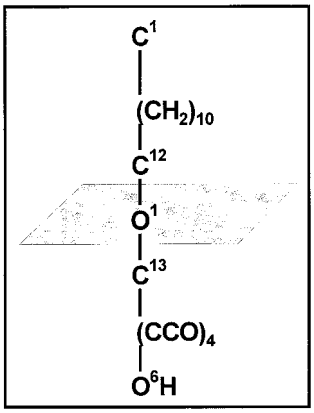

Figure 1. Numbering of carbon and oxygen atoms in the $C_{12}E_5$ surfactant molecule.

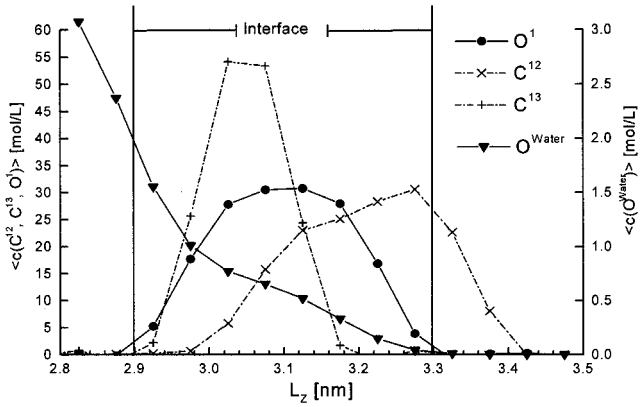

Figure 2. Average concentration profile of O^1, $C,^{12}$ C^{13}, and O^{Water} atoms in the direction of the vector representing the water surface normal.

data were calculated using the molecular dynamics program DISCOVER. This simulation program was developed by Molecular Simulation Inc., San Diego.[38]

Results

For further discussion of our results we first introduce the numbering of the carbon and oxygen atoms in the surfactant molecules (Figure 1). For reasons of simplifications we denote the simulation system of the 36 $C_{12}E_5$ monolayer as S36 and the previous simulated model consisting of 25 $C_{12}E_5$ surfactants[30] as S25.

The evaluation of structural properties such as orientation angles and layer thicknesses requires an appropriate definition of the water surface. Additionally, this definition is complicated on the grounds of the surface roughness. In Figure 2 the average concentration profile in the *z* direction for water oxygen atoms O^{Water} and the $C,^{12}$ C^{13}, and O^1 atoms of the surfactant molecules are summarized. The average concentration $\langle c_z \rangle$ was calculated from

$$\langle c_z \rangle = \frac{\Delta N_i}{N_A V_{Box}} \tag{1}$$

$\langle c_z \rangle$ represents the time average of the concentration in the *z* direction. ΔN_i is the amount of a specific atom *i* located in a small volume interval $\Delta V = \Delta L_z L_y L_x$ ($\Delta L_z = 50$ pm). N_A is Avogadro's constant, and V_{Box} denotes the total volume of the simulation box.

From Figure 2 it is evident that the average water oxygen concentration decreases to zero at 3.3 nm, and at $L_z = 2.9$ nm

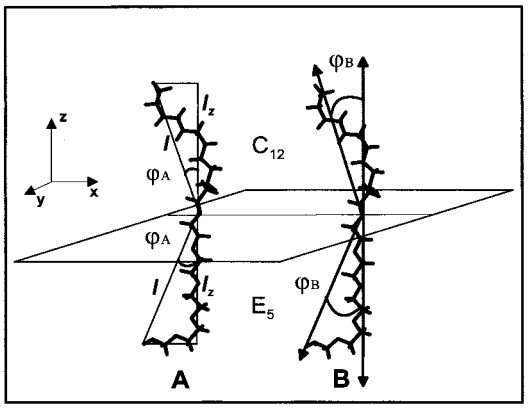

Figure 3. Definition of the tilt angle calculations.

$\langle c_z \rangle$ is about half of the water bulk density. On close inspection it was found that no water molecules evaporated in the gas phase beyond the L_z value of 3.3 nm. Following the suggestion of Schweighofer et al.,[22] we define the water surface by a plane lying between $L_z = 2.9$ and 3.3 nm. The surface plane was constructed by the best fit of all water oxygen atom positions in the range between half of the bulk density at 2.9 nm and vanishing water concentration at 3.3 nm. This means that with every stored configuration in the trajectory, the water surface was recalculated since the number of water molecules as well as their positions changed with every simulation time step. A detailed analysis showed that these changes were not significant to the angle between the *z* axis and the surface. It was observed that during the simulation the surface normal remained almost parallel to the *z* axis of the coordinate system. From Figure 2 it becomes clear that the O^1 oxygen atoms interact with the water surface since these atoms tend to be concentrated in the interface region. Also, the C^{13} atoms are mainly located in the interface region. The maximum of the C^{13} plot is shifted more toward the water phase (3.02 nm in comparison to the O^1 concentration profile curve, which has its maximum at 3.12 nm). It is worthwhile to mention that the C^{12} atom is also partially in contact with water molecules at the interface. In contrast to C^{13} the interaction between C^{12} and water is less distinctive and the maximum of the C^{12} curve lies at 3.28 nm. This is very close to that point where the water concentration decays to zero.

Chain Orientation at the Surface. The orientations of the hydrophobic alkyl chains and the hydrophilic glycol chains within the monolayer are of foremost interest for a detailed analysis of the adsorbed film. In Figure 3 two different methods for calculating the average tilt angle of the specific chains are presented. With procedure A the average tilt angle is calculated using

$$\cos \varphi = \frac{\langle l_z \rangle}{\langle l \rangle} \tag{2}$$

$\cos \varphi$ is obtained from the ratio of the chain layer thickness l_z and the variable *l*. The latter parameter denotes the distance between the mass center of the terminal hydrogens on C^1 with respect to the hydrogen atom connected on the terminal oxygen atom O^6 and the point of intersection of the relevant chain with the water interface. l_z is the projection of the chain in direction of the surface normal. In method B the average tilt angle is calculated from angles between appropriate vector definitions and the normal of the water surface. In the E_5 chains, vectors were constructed from the distance between the first oxygen atom O^1 and the terminal hydrogen atom connected to O.[6] In the C_{12} chains the vectors between C^{12} and the mass center of

TABLE 1: Average Tilt Angles and Chain Layer Width of the C_{12} and E_5 Chains[a]

chain	$\langle l \rangle$ (nm)	$\langle l_z \rangle$ (nm)	$\langle \varphi_A \rangle$ (deg)	$\langle \varphi_B \rangle$ (deg)
C_{12}	1.48 ± 0.03	1.05 ± 0.04	44.52 ± 3.4 (47.6 ± 5.2)	42.1 ± 2.9 (47.4 ± 3.8)
E_5	1.51 ± 0.01	1.48 ± 0.01	11.4 ± 4.8	10.5 ± 0.5 (11.3 ± 0.8)

[a] l and l_z are already corrected by the hydrogen van der Waals radius of 0.11 nm. In parantheses: simulation results of 25 surfactants adsorbed on the water surface (S25).

the terminal hydrogen atoms connected to C^1 were used for the calculation of tilt angles.

In Table 1 the calculated chain layer width and average tilt angles of the C_{12} and E_5 chains are summarized. It is evident that the C_{12} chains are tilted away with respect to the surface normal. We obtained values of about 42−44.5° depending on the definition of the tilt angle. The calculated average tilt angle from our previous simulation of the S25 system was of the order of 47°, which is in fairly good agreement with the S36 system.

Due to the parallel orientation of the E_5 chains, l and l_z have quite similar values. It is therefore difficult for this system to evaluate a precise tilt angle with method A. It turns out that l and l_z are very sensitive to statistical uncertainties. These fluctuations have their reason in the dynamically changing water oxygen positions. However, for the S36 system, $\langle \varphi \rangle$ calculated by procedure A is similar to the value obtained from the vector defintion B. The only difference is that method A suggests a larger standard deviation of ±4.8°. We can, hence, conclude that the simulation of 25 alkyl glycol ether surfactants on the air/water interface is already a suitable model for the evaluation of molecular orientation within the monomolecular $C_{12}E_5$ film. This is also supported by the fact that the calculated average tilt angles of the E_5 chains in the S25 and S35 system are very similar. Both systems indicate an almost parallel orientation of these chains in respect to the surface normal with a tilt angle value of about 10.5−11.4°.

Analysis of the Chain Conformation. Rotations around carbon bonds in the C_{12} and E_5 chains cause transitions of trans into gauche conformations and vice versa. To investigate the average chain conformations in the monomolecular film in more detail, a conformation distribution analysis was performed. Relevant results are summarized in Figure 4. It is evident that trans conformations are predominant in C_{12} and E_5 chains. A more detailed inspection reveals that the trans ratio is significantly larger in E_5 chains than in C_{12} chains. Furthermore, the maximum of the dihedral distribution of the gauche (+) conformations in the E_5 chains is shifted to a smaller value. Accordingly, the maximum of the gauche (−) plot is located at a larger dihedral angle.

In Figure 5 the average dihedral distributions of rotations around C−O and C−C bonds in the E_5 chains are presented. The average percentage distributions of the trans and gauche conformations were obtained from the curves in Figures 4 and 5 by integration of the dihedral distributions in the appropriate intervals between 0 and 120, 120 and 240, and 240 and 360°. The results are summarized in Table 2.

To summarize, we may state that the glycol ether chains are forced to keep their all trans configurations. In contrast to the E_5 chains trans to gauche transitions are more preferred in the C_{12} alkyl chain. The reason for this effect could be due to the formation of a hydrogen bond network, which tends to fix the E_5 oxygen atoms in certain positions. Consequently, rotations around C−C and C−O are strongly restricted within the E_5 chain. Indeed, the gauche ratio of 2% indicates that rotations

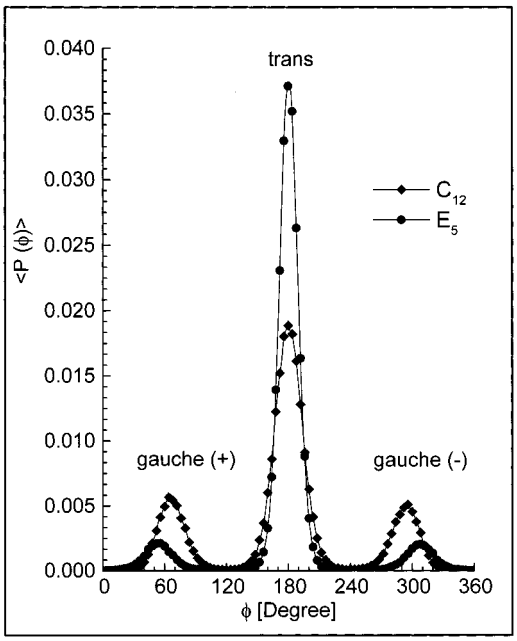

Figure 4. Average conformation distributions in the C_{12} and E_5 chains.

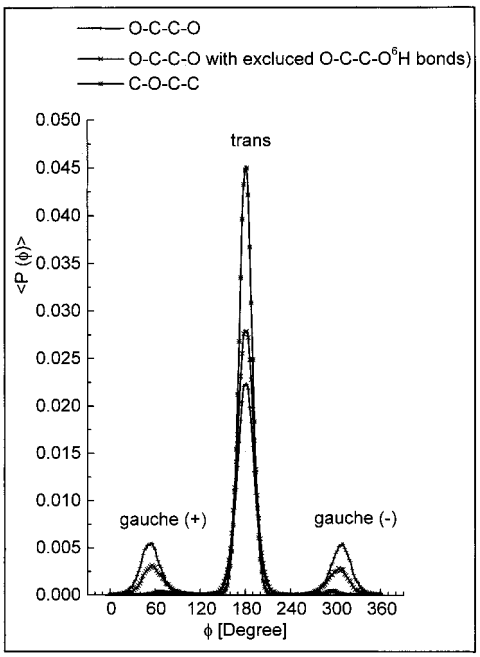

Figure 5. Detailed analysis of the average dihedral distributions with consideration of the C−C and C−O bonds in the E_5 chains.

TABLE 2: Average Percentage Dihedral Distributions Calculated by Integration of the Dihedral Distributions[a]

system	trans (%)	gauche (%)
C_{12}	64 (64)	36 (36)
E_5	86 (86)	14 (14)
E_5 (C−C−O−C)	98 (94)	2 (4)
E_5 (O−C−C−O)[b]	79 (84)	21 (16)
E_5 (O−C−C−O)[c]	63 (67)	37 (33)

[a] The results of the S25 system are given in paranthesis. [b] Without the terminal O−C−C−OH dihedral. [c] Terminal O−C−C−OH dihedral was included.

around C−O atoms seem to be unfavorable. The gauche ratio of rotations around the C−C bonds in the E_5 chains is about 37%. If rotations around the terminal O−C−C−OH bond are neglected, the gauche ratio decreases to 21%. This comparison

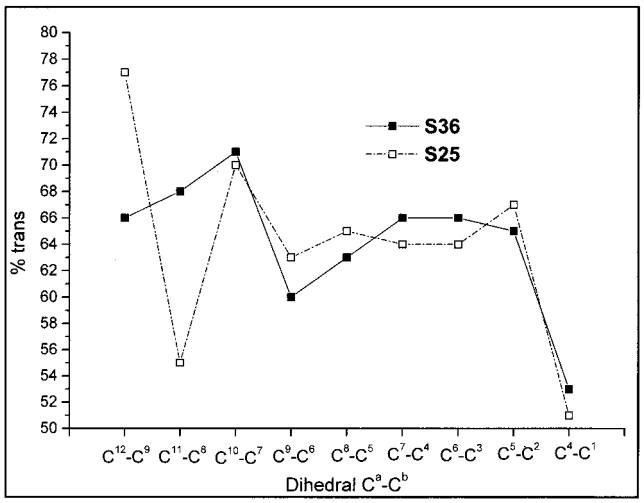

Figure 6. Percentage distribution of trans conformations of specific dihedrals in the C_{12} chain.

shows that a large contribution comes from rotations around the terminal bonds. The S25 and S36 simulation results are, again, in fairly good agreement.

Subsequently, we shall discuss the rotations of specific C−C bonds within the hydrophobic alkyl chain. A trans conformation analysis of specific dihedrals in the C_{12} chains is shown in Figure 6. Specific rotations around C^2-C^3 (dihedral C^4-C^1) lead to a low ratio of trans conformations. From this result it becomes clear that trans−gauche transitions occur frequently in the alkyl chain ends. The result is a large flexibility in this chain section. Obviously, trans to gauche transitions occurring at the chain ends distort the packed chains less than rotation around bonds in the central part of the molecules. The results of the S36 and S25 system show a distinctive deviation of the $C^{12}-C^9$ and $C^{11}-C^8$ dihedrals. Presently, the reason for this discrepancy is not clear. Nevertheless, both simulations suggest a slightly preferred trans to gauche transition in the C^9-C^6 dihedral.

It can be concluded that tilt angles calculated from chain layer width can be wrong. This phenomenon is due to the chain end flexibility, which tends to reduce the chain lengths. Consequently, larger tilt angles can be deduced. This fact becomes obvious from the molecular structure of the surfactants adsorbed on the water surface displayed in Figure 7. It is easy to see the different orientations of the C_{12} and E_5 chains. It can also be recognized that the alkyl chains are more fluid like. In contrast, the E_5 chains are oriented perpendicular to the water surface, except for the terminal chain segments. These parts of the molecules are more parallel aligned with respect to the water surface.

Mobility of the Alkyl and Glycol Ether Chains. A different mobility of the chains or the chain segments can be derived from the results of the conformation distribution. This analysis includes the calculation of the chain orientation with respect to the surface. In Figure 7, the different chain mobility also becomes evident.

The mobilities of chain segements and atoms located at different parts in the C_{12} and E_5 chains can be calculated from the mean square displacement correlation function defined in

$$\mathrm{MSD}(t) = \frac{1}{N}\sum_{i=1}^{N}\langle[\mathbf{r}_i(t) - \mathbf{r}_i(0)]^2\rangle \qquad (3)$$

Here, $\mathbf{r}_i(t)$ denotes the position vector of particle i and N is the number of particles. This formula describes the average of the mean square displacement of particle i calculated from all particle positions of the trajectory. In this context a particle position can be either a position of an atom or it describes a center of mass of a defined atom set. From the atom positions stored in the trajectory data file, we calculated the average mean square displacements of the mass centers of the alkyl and glycol ether chains. We have also analyzed the mobility of different chain sections while the average mean square displacements of the C^1, O^1, C^{13}, and O^6 atoms were determined. Relevant results are plotted in Figure 8.

It turns out that the large mobility of the alkyl chain ends results from the slope of the MSD-C^1 plot. The mobility of the mass center of the C_{12} chains is also remarkable. In contrast,

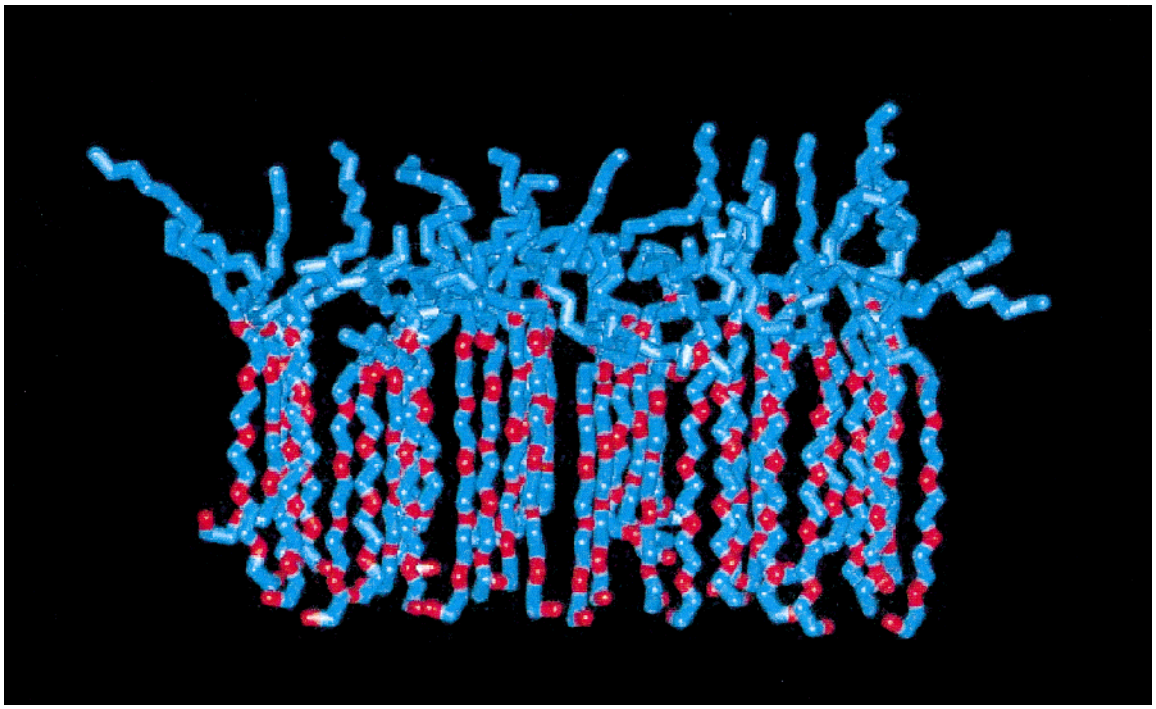

Figure 7. A Representative molecular structure of the $C_{12}E_5$ surfactant molecules adsorbed on the water surface. The Cartesian coordinates are extracted from the trajectory at a simulation time of 900 ps. For a better clarity, the water molecules are not printed.

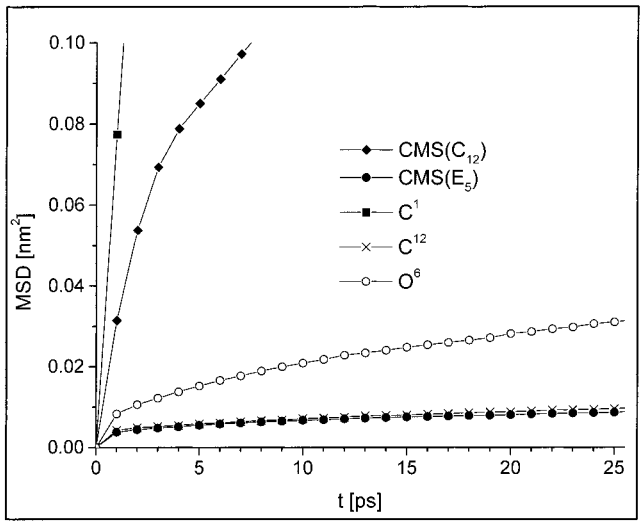

Figure 8. Average mean square displacements of the C_{12} and E_5 mass center and for the C^1, C^{12}, and O^6 atoms.

the mobility of the C_{12} chains in the vicinity of the water surface is very low. The MSD plot of the mass centers of the E_5 chains shows that the flexibility of the polar headgroups is strongly restricted in the water phase. Merely the E_5 chain ends exhibit a larger degree of mobility. To summarize, we may conclude that the $C_{12}E_5$ surfactants are anchored at the water surface by the glycol chains. Lateral diffusion of the surfactant molecules could not be observed. This holds at least for the simulated time interval of 1 ns.

Structure of the Glycol Ether Chains. The results of the chain mobility analysis show that, with the exception of the E_5 chain ends, the atoms must be ordered to a large extent in the midchain section. To determine the average structure of the E_5 chains, we calculated several oxygen−oxygen pair distribution functions (PDF's). From these data the average coordination number $\langle n_{ab}(r)\rangle$, defined in eq 4,

$$\langle n_{ab}(r)\rangle = \rho_b \int_0^r g_{ab}(r) 4\pi r^2 \, dr \tag{4}$$

can be calculated. $g_{ab}(r)$ denotes the PDF between atoms a and b, ρ_b is the bulk density and the term $4\pi r^2 \, dr$ represents the volume element dV measured at a distance r from the central atom. The integral refers to the first peak, up to the position of the first minimum. $g_{ab}(r)$ is simply obtained by computing the average local density of type b atoms around a type a atom in a specific shell volume element.

$$g_{ab}(r) = \frac{\Delta\langle N_{ab}(r)\rangle}{\rho_b \Delta V(r)} \tag{5}$$

$\Delta\langle N_{ab}(r)\rangle$ is the average number of type b atoms at the distance between r and $r + \Delta r$ from a type a atom. ΔV denotes the shell volume. The calculation of $g(r)$ and $n(r)$ between the oxygen atoms assembled within the same layer (O_1- -O_1, O_2- -O_2, ..., O_6- -O_6) provides information on the phase structure of the E_5 chain.

In Figures 9 and 10 the $g(r)$ and $n(r)$ functions are plotted. The relatively broad pair distributions of the O_1-O_1 and O_6-O_6 oxygens show that these atoms are not well ordered in the specific layer. Conversely, narrow and pronounced peaks with a maximum of about 750 pm are charcteristics of the O_2-O_2, O_3-O_3, and O_4-O_4 PDF's. It is evident that these oxygen atoms

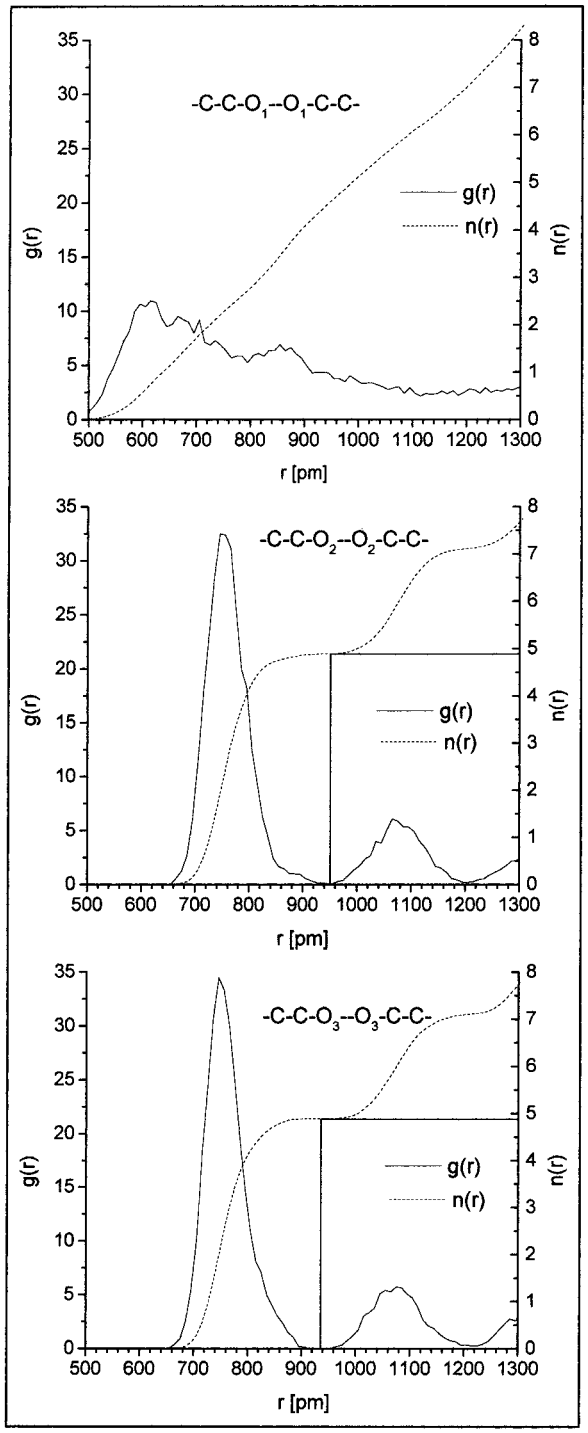

Figure 9. Average pair distribution functions beween E_5 oxygens (O_1, O_2, O_3) arranged in a common layer.

are well ordered. The significant maximum at 750 pm indicates the average distance between oxygen atoms in the layer. The weak peaks in the $g(r)$ plots at a maximum of 1080 pm correspond to oxygen atoms in the second shell. From the coordination number function it can be concluded that the average number of nearest oxygen atoms is in the range of 5. The O_5 atoms are less structured than O_2, O_3, and O_4 since the first peak becomes smaller and broader. Due to the high flexibility of the E_5 chain ends, the structural behavior of O_5 and O_6 is not surprising. The high flexibility results in a less ordered structure.

Typical patterns of the layers formed by the oxygen atoms are plotted in Figures 11−13 at different simulation times. At

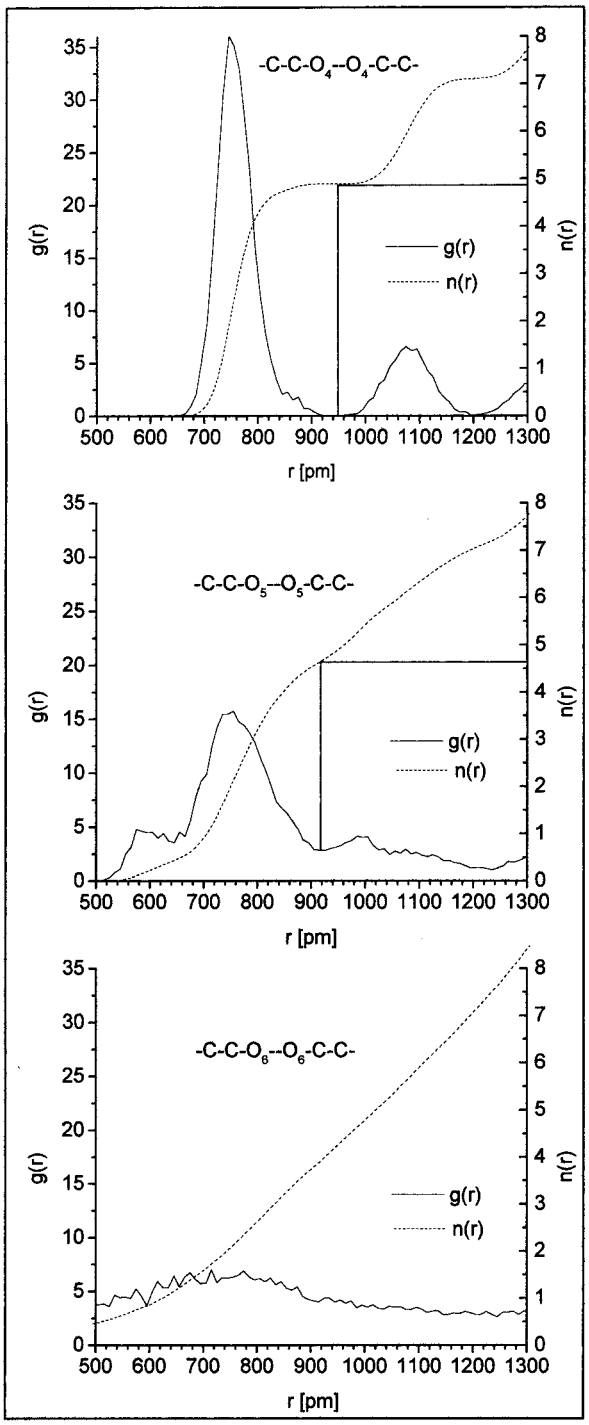

Figure 10. Average pair distribution functions beween E_5 oxygens (O_4, O_5, O_6) arranged in a common layer.

the beginning of the computer simulation the oxygen atoms of the E_5 chain were arranged in such a way that each oxygen layer forms a rectangular lattice of equal size. According to the surfactant surface concentration of 0.55 nm^2/molecule the average distances between the oxygen atoms were equal to 740 pm. The degree of lattice deformation shown in Figures 11−13 is a consequence of the motion of oxygen positions in the layer. The observed lattice deformation of the O_6 and also O_1 layers can be explained by the flexibility of the E_5 chain ends. It is interesting to note that within the time regime of 500−1000 ps, each pattern in the O_1−O_6 series remains stable. This is an indication that the system has reached equilibrium conditions.

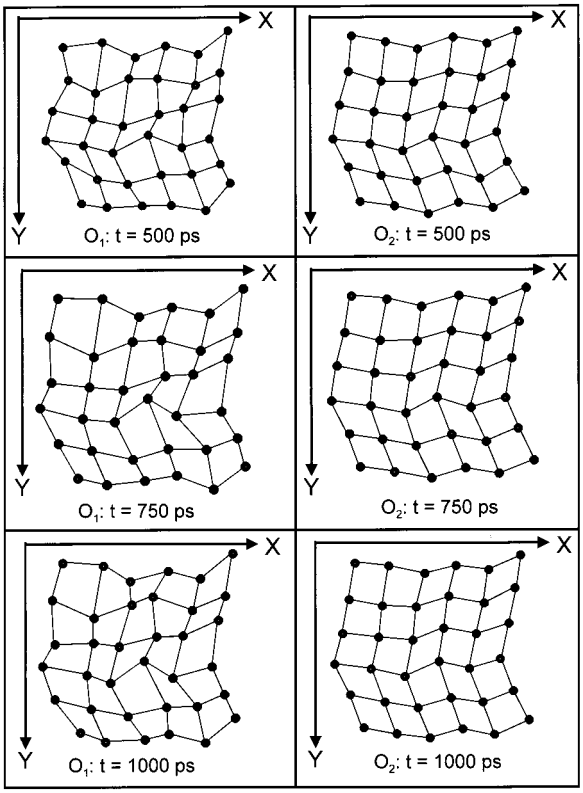

Figure 11. O_1 and O_2 patterns at simulation times of 500, 750, and 1000 ps.

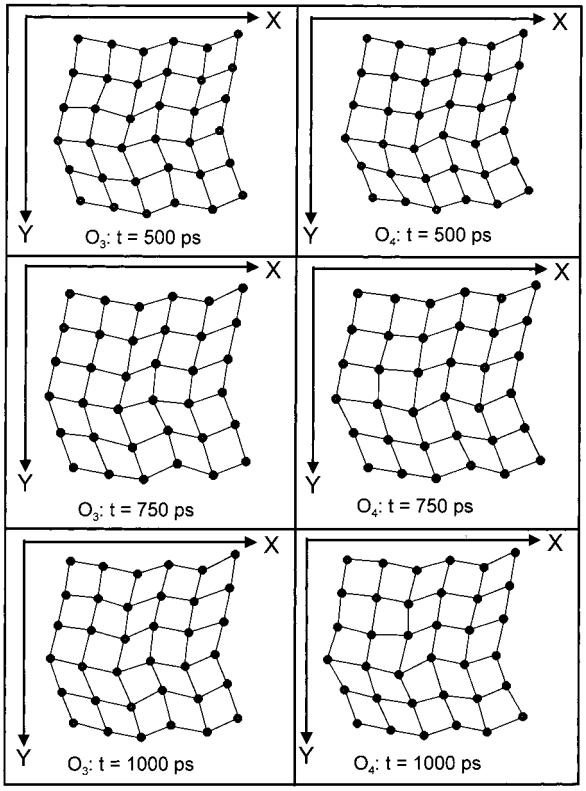

Figure 12. O_3 and O_4 patterns at simulation times of 500, 750, and 1000 ps.

To get information on the molecular arrangement of the O_2, O_3, and O_4 oxygen atoms in the layer, we constructed circles around specific oxygen atoms. These regions were drawn with a radius of 750 pm, which represents the largest probability of finding other adjacent oxygen atoms at this distance (Figures 9

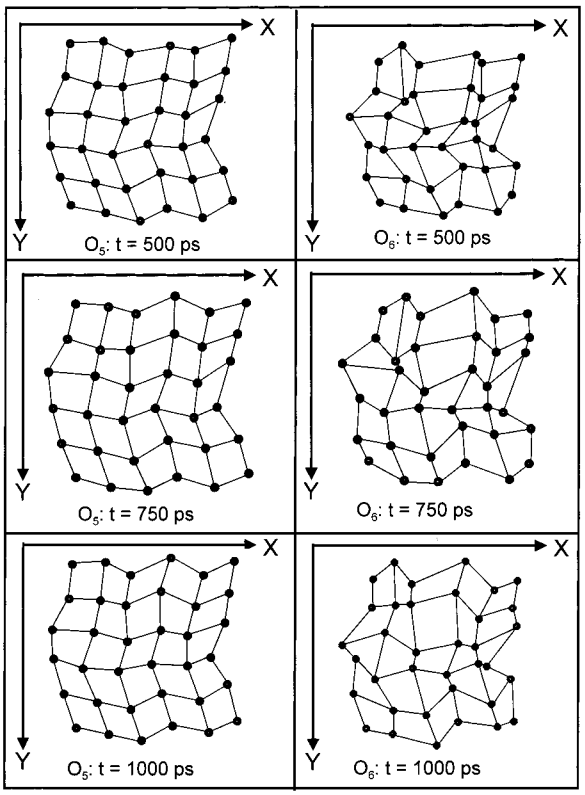

Figure 13. O_5 and O_6 patterns at simulation times of 500, 750, and 1000 ps.

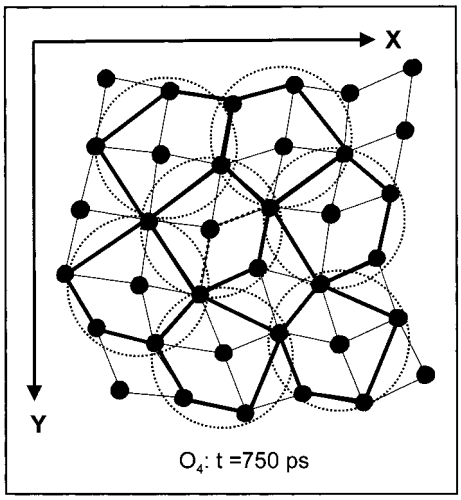

Figure 14. Pentagonal structure of oxygens in the E_5 chain presented on the O_4 layer at a simulation time of 750 ps.

and 10). Afterward, we connected all oxygen atoms located on the circle border and inside the circle area. Typical results for the O_4 layer at a simulation time of 750 ps are presented in Figure 14. The pair distribution functions and the graphic structure in Figure 14 point to the existence of a pentagonal arrangement of oxygen atoms in the highly ordered inner segments of the E_5 chain. Two overlapping pentagons are shown in Figure 14, and this region is expressed by dotted lines.

Discussion and Conclusions

With molecular dynamics simulations we have calculated tilt angles of the C_{12} and E_5 chains. We can conclude that the alkyl chains are fluid-like with an average tilt angle of approximately 43°. Conversely, the E_5 chains are more ordered and aligned perpendicular to the surface plane. From the analysis of the molecular structure, from the conformation distribution, and from the calculation of the mean square displacements in different chain sections, a high degree of flexibility of the terminal groups in the C_{12} and E_5 chains becomes evident. In comparison to E_5, the hydrophobic C_{12} chains are considerably less ordered. From the comparison between the simulation systems of 25 and 36 surfactants it can be concluded that already 25 $C_{12}E_5$ molecules were sufficient for the calculation of detailed structural properties such as molecular orientation on the air/water interface.

In the investigated concentration regime the alkyl chains of the $C_{12}E_5$ surfactants are not densely packed. From comparisons with molecular dynamics simulations of long-chain surfactants adsorbed on the air/water surface in the same surfactant concentration regime, it can be concluded that the molecular orientation of the C_{12} chain is similar to surfactants with linear hydrophobic chains and small polar headgroups. Karaborni et al.[7] found that monolayer tilts of single chain surfactants varied from 10 to 36° with increasing area/molecule. Other simulations of long-chain surfactants revealed that the mean tilt angle varied from 40 to 60°.[12] In *n*-hexadecyltrimethylammonium chloride monolayers the average tilt angle was found to be of the order of 40°.[24] Generally, the simulations of long-chain model surfactants revealed that an increase of the molecular area caused an increase of the average tilt angle.[11,15]

The result of the enhanced C_{12} chain end flexibility was also observed in simulations of long-chain surfactants. It was found that most of the gauche conformations occurred around bonds near the hydrophobic chain ends.[7,15,19]

Despite the similarities concerning the hydrophobic chain orientation, there seems to be a difference in the diffusion behavior between surfactants with small headgroups and amphiphilic alkyl glycol ethers. In a previous simulation the diffusion constant of *n*-hexadecyltrimethylammonium chloride in the monolayer was calculated to 1.9×10^{-6} to 4.8×10^{-6} cm^2/s.[24] Karaborni et al. discussed growing diffusion with increasing molecular area to a maximum of 1.6×10^{-5} cm^2/s. This holds for a surface area of 0.30 nm^2/molecule.[7] Conversely, we observed strong anchored alkyl glycol ether headgroups at the water surface. Our results imply a restricted mobility of the E_5 chains. The discrepancy can be explained by a network of hydrogen bonds that tends to freeze the monolayer structure. It is, therefore, very interesting to analyze the nature and strength of hydrogen bonds between the E_5 chains. This work is still in progress.

From the calculations of pair distribution functions between E_5 oxygen atoms arranged in a common layer, we could show that O_1 and O_6 oxygens are not well ordered whereas the oxygen atoms in the midsections of the E_5 chains showed a pronounced structure referring to the atomic arrangement in the layer. Furthermore, the pair distribution functions and the pattern analysis revealed a pentagonal arrangement of oxygen atoms in this highly ordered inner segment of the E_5 chains.

In recent studies of the packing structures in monolayers of partially fluorinated amphiphiles[14,16−18] and tetradecyltrimethylammonium bromide monolayers a hexagonal surfactant arrangement was found.[24] These results cannot directly be compared with the pentagonal structure of glycol ether chains obtained from our simulation because the discussed atomic arrangements are highly sensitive to the surfactant concentration and the mobility of the surfactants on the water surface. The mobility of the glycol ether chains are rather different from ionic surfactants with relatively small headgroups. It is, however, also

interesting to study the adsorption properties of the glycol ether chains as a function of the surfactant concentration. This work is still in progress.

An important conclusion from the diffusion behavior of the surfactants in the monolayer is that the investigation of structural properties of the alkyl chains needs no explicit consideration of water molecules in the simulation model. The model could be simplified by grafting the surfactants on a planar surface. With this procedure the enhanced simulation of phase transitions within the monolayer seems to be possible,[39] provided that no significant structural transitions in the alkyl or glycol ether chains appear. The discontinuity of the average total energy with dependence on the molecular area should then give information on liquid-condensed (LC) to liquid-expanded (LE) and LE to gas (G) phase transitions. However, this idea of a successful simulation without using solvent molecules has still to be proven.

Another topic of actual relevance is the molecular behavior of alkyl glycol ether surfactants in the highly dilute concentration regime. Since no interactions appear with neighboring molecules in this system, the interaction between the alkyl chains and the water molecules on the surface should be of major importance for the molecular structures at the air/water interface. Such types of investigation are still in progress.

Although a small number of surfactant molecules are sufficient to calculate tilt angles, it was not really clear whether the system size was sufficient for calculation of other collective interface properties. Recently, Karaborni and Siepmann performed several computer simulations to study the effect of system size on the structure of model surfactant monolayers.[5] It was concluded that system size effects on collective interface properties are important at least in the regime of intermediate surfactant concentrations. To solve this problem, system-size effects on nonionic and water-soluble C_mE_n surfactants on the air/water interface have to be systematically investigated.

Acknowledgment. Financial support of this work by grants of the Deutsche Forschungsgemeinschaft (DFG: Re 681/4-3; Graduate Research Project; "The Improvement of the Water Cycle in Urban Areas for the Protection of Soil and Groundwater") and the *Forschungspool* of the University of Essen are gratefully acknowledged. We thank Mrs. S. Vogt for writing and providing some very useful UNIX shell scripts. We would also like to thank the Computer center of the University of Essen for interesting discussions and technical assistance.

References and Notes

(1) Lu, J. R.; Hromadova, M.; Thomas, R. K.; Penfold, J. *Langmuir* **1993**, *9*, 2417.

(2) Lu, J. R.; Li, Z. X.; Thomas, R. K.; Staples, E. J.; Tucker, I.; Penfold, J. *J. Phys. Chem.* **1993**, *97*, 8012.

(3) Lu, J. R.; Li, Z. X.; Thomas, R. K.; Staples, E. J.; Thompson, L.; Tucker, I.; Penfold, J. *J. Phys. Chem.* **1994**, *98*, 6559.

(4) Lu, J. R.; Li, Z. X.; Thomas, R. K.; Binks, B. P.; Crichton, D.; Fletcher, P. D. I.; McNab, J. R.; Penfold, J. *J. Phys. Chem. B* **1998**, *102*, 5785.

(5) Karaborni, S.; Siepmann, J. I. *Mol. Phys.* **1994**, *83*, 345.

(6) Karaborni, S. *Langmuir* **1993**, *9*, 1334.

(7) Karaborni, S.; Toxvaerd, S. *J. Chem. Phys.* **1992**, *96*, 5505.

(8) Karaborni, S.; Toxvaerd, S.; Olsen, O. *J. Phys. Chem.* **1992**, *96*, 4965.

(9) Karaborni, S.; Toxvaerd, S. *J. Chem. Phys.* **1992**, *97*, 5876.

(10) Karaborni, S.; Verbist, G. *Europhys. Lett.* **1994**, *27*, 467.

(11) Bareman, J. P.; Klein, M. L. *J. Phys. Chem.* **1990**, *94*, 5202.

(12) Bareman, J. P.; Cardini, G.; Klein, M. L. *Phys. Rev. Lett.* **1988**, *60*, 2152.

(13) Cardini, G.; Bareman, J. P.; Klein, M. L. *Chem. Phys. Lett.* **1988**, *145*, 493.

(14) Shin, S.; Collazo, N.; Rice, S. A. *J. Chem. Phys.* **1993**, *98*, 3469.

(15) Buontempo, J. T.; Rice, S. A.; Karaborni, S.; Siepmann, J. I. *Langmuir* **1993**, *9*, 1604.

(16) Shin, S.; Collazo, N.; Rice, S. A. *J. Chem. Phys.* **1992**, *96*, 1352.

(17) Collazo, N.; Shin, S.; Rice, S. A. *J. Chem. Phys.* **1992**, *96*, 4735.

(18) Collazo, N.; Rice, S. A. *Langmuir* **1991**, *7*, 3144.

(19) Harris, J.; Rice, S. A. *J. Chem. Phys.* **1988**, *89*, 5898.

(20) Bishop, M.; Clarke, J. H. R. *J. Chem. Phys.* **1991**, *95*, 540.

(21) Siepmann, J. I. *Prog. Colloid Polym. Sci.* **1997**, *103*, 280.

(22) Schweighofer, J.; Essmann, U.; Berkowitz, M. *J. Phys. Chem. B* **1997**, *101*, 3793.

(23) Böcker, J.; Schlenkrich, M.; Nicklas, K.; Brickmann, J.; Bopp, P. *J. Phys. Chem.* **1992**, *96*, 9915.

(24) Tarek, M.; Tobias, D. J.; Klein, M. L. *J. Phys. Chem.* **1995**, *99*, 1393.

(25) Pohorille, A.; Benjamin, I. *J. Phys. Chem.* **1993**, *97*, 2664.

(26) Pohorille, A.; Benjamin, I. *J. Chem. Phys.* **1991**, *94*, 5599.

(27) Gao, J.; Jorgensen, W. L. *J. Phys. Chem.* **1988**, *92*, 5813.

(28) Sokhan, V. P.; Tildesley, D. J. *Faraday Discuss.* **1996,** *104*, 193.

(29) Michael, D.; Benjamin, I. *J. Phys. Chem. B* **1998**, *102*, 5145.

(30) Kuhn, H.; Rehage, H. *Tens. Surf. Det.* **1998**, *35*, 448.

(31) Weiner, S. J.; Kollmann, P. A.; Nguyen, D. T.; Case, D. A. *J. Comput. Chem.* **1986**, *7*, 230.

(32) Weiner, S. J.; Kollmann, P. A.; Case, D. A.; Singh, U. C.; Ghio, C.; Alagona, G.; Profeta, S.; Weiner, P. *J. Am. Chem. Soc.* **1984**, *106*, 765.

(33) Weiner, P. K.; Kollmann, P. A. *J. Comput. Chem.* **1981**, *2*, 287.

(34) Berendsen, H. J. C.; Postma, J. P. M.; van Gunsteren, W. F.; Hermans, J. In *Intermolecular Forces*; Pullman, B., Ed.; Reidel: Dordrecht, Holland, 1981; p 331.

(35) Press, W. H.; Flannery, B. P.; Teukolsky, S. A.; Vetterling, W. T. *Numerical Recipes*; Cambridge University Press: London, New York, 1986.

(36) Ryckaert, J.-P.; Cicotti, G.; Berendsen, H. J. C. *J. Comput. Phys.* **1977**, *23*, 327.

(37) Verlet, L. *Phys. Rev.* **1967**, *159*, 98.

(38) Molecular Simulation Inc. DISCOVER Ver. 3.0.0, San Diego, 1996.

(39) Collins, S. J.; Dhathathreyan, A. *J. Colloid. Interface Sci.* **1998**, *203*, 249.